Evolution of the Cu $K\alpha_{3,4}$ satellites from threshold to saturation

M. Fritsch,[1] C. C. Kao,[2] K. Hämäläinen,[3] O. Gang,[1] E. Förster,[4] and M. Deutsch[1]
[1]*Physics Department, Bar-Ilan University, Ramat-Gan 52900, Israel*
[2]*NSLS, Brookhaven National Laboratory, Upton, New York 11973*
[3]*Physics Department, FIN-0014 Helsinki University, Helsinki, Finland*
[4]*Institute for Optics and Quantum Electronics, Friedrich Schiller University Jena, D-07743 Jena, Germany*
(Received 17 September 1997)

Photoexcited Cu $K\alpha_{3,4}$ satellite spectra were measured as a function of excitation energy, from threshold at ~10.010 keV to saturation at ~11 keV. A two-regime behavior is found, where in the near-threshold regime (TR) both the shape and the intensity of the spectrum vary. In the higher-energy regime (GR) only the intensity varies but not the shape. The GR spectra are well described by relativistic Dirac-Fock calculations. The analytic Thomas model, applicable in this adiabatic regime, does not agree well with the measured intensity variation with excitation energy. The continuous intensity rise from zero at threshold confirms the shake theory prediction of a pure shake-off process for inner-shell, medium-Z atom satellites. The thresholds for the individual spectral features, the overall shape variation, and the variations of the individual lines in the TR regime are determined, and discussed. [S1050-2947(98)01003-8]

PACS number(s): 32.30.Rj, 32.70.−n, 32.80.Fb

I. INTRODUCTION

Ionization and excitation processes in inner-shell electrons far above threshold have been extensively studied [1]. They are well described theoretically by the prevailing sudden or frozen core approximation, whereby the ejected electron is removed immediately, the atom's shell structure is kept frozen in its ground-state configuration, and the electrons treated as independent, noninteracting particles [2]. The excitation and deexcitation processes can be then conveniently treated as two independent, and consecutive, processes. However, the closer one gets to the energetic threshold for the specific excitation, the worse these approximations become. Effects like intershell and intrashell electronic correlations, the gradual relaxation of the atomic shells, and the changing interaction between the slow-moving ejected electron and the relaxing atom assume increasing importance and even dominance near threshold [2,3]. Furthermore, the excitation process, and the deexcitation by (x-ray) photon or (Auger) electron ejection can no longer be considered as independent processes; they become increasingly simultaneous, and mutually interacting. This regime is known as the adiabatic excitation limit [4], since the atomic structure relaxes adiabatically in response to the inner-shell excitation, over a time scale comparable with that required for the slow-moving ejected electron to leave the atom. Thus, the near-threshold region provides, in principle, a unique opportunity for studying these interesting and important effects, which go beyond the prevailing sudden approximation-independent particle models of the excitation–deexcitation processes and of the structure of atoms.

Intershell and intrashell correlations in an atom are expected to have a particularly large impact on satellite spectra, which originate in multielectronic transitions in the same atom. In the sudden approximation, high-excitation-energy limit these spectra were mostly assigned to, and studied within, shake theory [2,5–8]. Shake theory predicts, however, a considerable variation of the excitation cross section from threshold up, since complete adiabatic relaxation implies no shakeup [9], while in the sudden limit shakeup satellites carry considerable intensity. A prominent theoretical approach to the calculation of the cross-section energy dependence in the adiabatic regime and its crossover to the sudden limit, pioneered by Thomas [4,9–11], employs time-dependent perturbation theory to describe the relaxation of the atom and its interaction with the slow moving photoelectron. The theory had some success in describing the cross section variation with excitation energy, and, in particular, its fast saturation close to the threshold in the very few then-available measurements on Ne and N_2, and in several later studies [12]. However, with very few exceptions [13], the majority of the more recent results address, almost exclusively, photoelectron satellite spectra associated with *valence* photoionization. Most of these results are at odds with the predictions of the Thomas model, indicating that these satellites are not dominated by shake processes but rather by a variety of other correlation effects [14,15]. As pointed out by Heiser *et al.* [15], the importance of shake processes in the production of satellites is expected to become increasingly dominant with increasing atomic number, and decreasing shell number. The Thomas model would be expected, therefore, to be more successful in describing shake processes accompanying K shell ionization in medium-Z atoms. It was indeed found to be so in the recent study of the K-shell satellites of Ar by Heiser *et al.* The K shell of medium- and high-Z atoms are, however, less accessible to threshold electron spectroscopy, and no suitable studies in this region are available at present.

Near-threshold x-ray emission spectroscopy, which should, in principle, allow one to study x-ray satellites in this region conveniently, was hampered until very recently by the lack of suitable excitation sources that are tunable, narrow-band, and intense enough to allow studying these weak transitions. With the recent development of synchrotron-based beamlines equipped with efficient, high-resolution fluorescence spectrometers over the last few years [16,17], detailed studies of this kind became possible [3,18,19]. For various

reasons, however, almost all the threshold x-ray emission spectra studied to date are in the soft x-ray region and address the low-binding-energy valence electron satellites in low-Z atoms [20]. As their electron spectroscopy counterparts, these spectra are strongly influenced by several competing effects such as initial- and final-state configuration interactions, interchannel coupling, and, most of all, multiatomic band-structure effects, which make the extraction of information on the basic single-atom shake-up–shake-off processes extremely difficult [2]. Since theory predicts a strong variation of the relative shake-off–shake-up probability with atomic and shell numbers [6,8], a study of the individual effects should be possible by a judicious choice of these two numbers. This was demonstrated by two pioneering studies. The first, by Armen *et al.* [21], studied the M-shell Auger satellite spectra in K-shell-photoexcited Ar, and allowed one to follow the evolution of the shake processes near threshold, although the separation into shakeup and shakeoff contributions was hampered by an $\sim$25% admixture of the shakeup in the larger shakeoff line. The second, by Krause and Caldwell [22], addressed the Be $1s$ photoionization, where the predominance of the $1s(2s2p)$ (conjugate) shakeup process, yielding an intensity as large as 40% of the diagram line, allowed its study in an almost pure state. Here we explore the other limit, not hitherto studied, of an almost pure shakeoff process [23]. The spectrum chosen for this study, the Cu $K\alpha_{3,4}$ satellites, originates in $\underline{2l}$ electron shake processes accompanying the $\underline{1s}$ photoionization. (In the following, underlining denotes hole states.) This choice, involving deep core levels in a medium-Z atom, should not only provide for an almost pure shake-off process, but should also eliminate effectively contributions from multiatomic, nonlocalized band-structure effects, which dominated virtually all previous valence-shell satellite studies. It should also provide a stringent test of adiabatic-regime theories, in particular that of Thomas [9,10], under conditions where they are expected to be valid.

In this study x-ray photoexcitation by monochromatized synchrotron radiation was employed to study the variations in the Cu $K\alpha_{3,4}$ emission spectrum (ranging from 8060 to 8100 eV) upon varying the exciting photon's energy, $E_{\text{excitation}}$, from the shake process' threshold at $\sim$10 000 eV up to the saturation of the satellite spectrum intensity at 11 200 eV. The results confirm the pure shakeoff nature of the spectrum, as predicted by theory. They also reveal two distinct regimes in the spectral evolution. In the first, up to $\sim$70 eV above threshold, the spectral shape as well as the overall intensity undergo a rapid and complicated variation with $E_{\text{excitation}}$, due to the slightly different thresholds for the various overlapping lines comprising the spectrum, and their different growth rates. In the second regime, from $\sim$70 to $\sim$1000 eV above threshold, no variation of the spectral shape is observed, and only the overall intensity increases monotonically to saturation at the range's upper end. The fully developed spectral shape is found to be in good agreement with *ab initio* relativistic Dirac-Fock (RDF) calculations, which allows one to identify the various spectral features with specific transitions. The predictions of the Thomas adiabatic model [9,10] show only partial agreement with the experimental results, indicating the need for further work.

II. EXPERIMENT

A. Introduction

The low intensity of the $K\alpha_{3,4}$ satellites, only $I(K\alpha_{3,4})/I(K\alpha_1)\approx 0.6\%$ [3,24,25], which, in turn, requires a high-intensity exciting beam, and the need for energy tunability mandate the use of a synchrotron source for these photoexcitation measurements. Even so, to obtain reasonable sampling times, a wiggler beamline had to be used in the measurements presented here. The fluorescence radiation was analyzed using a Johan-type Rowland circle spectrometer, followed by an intrinsic Ge detector, to obtain a high signal-to-noise ratio. We now discuss in some detail the various components of the experimental setup, the methods used in analyzing the data, and some aspects of the *ab initio* calculations.

B. Measurement setup and procedures

The measurements were done at the wiggler beamline X25 at NSLS, Brookhaven National Laboratory [16]. The beamline optics include a focusing toroidal mirror and either a Si(111) or Si(220) double crystal monochromator providing a primary resolution from $\sim$1 to $\sim$7 eV, depending on slit settings. In our measurements a 3–4-eV resolution was employed resulting in a flux of $(5–7)\times 10^{11}$ photons/sec in a spot size of ~ 1 mm^2. The primary intensity was monitored in front of the sample by an ionization chamber, and used to normalize the data. The sample was a polycrystalline high-purity Cu foil 25.4 μm thick. The fluorescence spectrometer employed the Johann geometry with a Rowland circle of 1 m diameter on a horizontal plane, and a spherically bent 3-in.-diameter Si(444) crystal. At the emission energy, $\sim$8080 eV, the high Bragg angle of the analyzer, $\sim$78°, provided an intrinsic resolution of 0.1–0.2 eV. Incidence and detection angles were fixed at 45° each, relative to the sample's surface. The consequent 90° scattering angle provided high immunity against scattered background radiation, due to the high degree of the horizontal linear polarization of the synchrotron radiation. The background was further reduced by using a nitrogen cooled Ge detector, having a $\leqslant$250-eV resolution, and an evacuated beam path from the sample to the detector.

Two different types of scans were done. In the first, denoted inscan in the following, the analyzer energy was fixed at that of one of the features in the spectrum, and the excitation energy $E_{\text{excitation}}$ was scanned across a predetermined range by varying the monochromator's Bragg angle. This allowed a convenient detection of the threshold energy for the given feature. In the second type, denoted outscan, $E_{\text{excitation}}$ was kept fixed, and the emission energy E_{emission} was scanned by varying the Bragg angle of the analyzer. This measurement produced a spectrum of the satellite lines, and was repeated for several incident energies in the range of interest. Several ancillary measurements were also done, such as scans of the $K\alpha_{1,2}$ spectrum, which was required for removing the contribution of the diagram lines at the position of the satellites, and for calculating relative intensities. The absolute energy scale of $E_{\text{excitation}}$ was calibrated, and checked periodically throughout the experiment, by measur-

ing the conveniently located Zn K-edge absorption spectrum ($E_K = 9660.7$ eV).

C. *Ab initio* transition calculations

The calculations were done using the relativistic Dirac-Fock (RDF) package GRASP [26], with supplementary code written in-house. Previous studies [27,28] indicate that in the frozen-core–sudden approximation limit it is important to take into account the rearrangement and full relaxation of the excited atom prior to the emission process. This is done by generating in all cases the initial- and final-state wave functions in separate, single configuration runs where the wave functions and energies of *all* orbitals are allowed to vary. The energies of the individual transitions are then obtain by subtracting the appropriate level energies, as calculated in the initial- and in the final-state calculations. The relative transition probabilities within each multiplet can be calculated by GRASP only when the wave functions of the initial and final states are orthogonal. This is not the case here, since the initial and final states were generated in separate runs. Thus, configuration interaction calculations were carried out to obtain the various transition probabilities using once the initial-state orbitals and again those of the final state. All the significant transition probabilities agreed with each other in the two sets to within $\pm 10\%$. In the fits discussed below line strengths calculated from the initial state wave functions were used, after verifying that those calculated using the final-state wave functions result in only insignificant deviations from the results presented below. This approach amounts practically to using the frozen-atom approximation to calculate the line strengths within each multiplet. The implications of this are discussed below. For further details on the calculations see Ref. [28].

D. Data treatment

Each raw measured spectrum was first normalized by the corresponding incident beam monitor counts (corrected for its $E_{\text{excitation}}^{-2}$ efficiency dependence) then all the outscans (inscans) for the same $E_{\text{excitation}}$ (E_{emission}) were summed to a single spectrum, the angular scale of which was converted to an energy scale, and the intensities corrected for the variation with energy of the self-absorption in the target foil of the emitted photons [29]. An additional correction due to the small energy dependence of the $K\alpha$ photoexcitation over the range measured was also applied [30]. These corrections were applied to both the inscans and outscans. For the outscans, the highly sloping $K\alpha_1$ tail underlying the satellite spectrum was subtracted off using a Lorentzian tail fitted to the $K\alpha_1$ line in energy ranges above and below the satellites region. The Lorentzian tail included contributions from the two Lorentzians conventionally used for an analytic representation of the $K\alpha_1$ line [28,31]. Care was taken not to obliterate any of the satellite-related features. The $K\alpha_1$ subtraction was complicated by the nonmonotonic, though very weak, intensity variations above 8090 eV, outside the satellite region, the origin of which is unclear at present. For spectra taken very close to threshold, where the intensity is low, this structure affected also the resolution of the spectra into individual Lorentzians (see below) and this region was, therefore, excluded from the fits.

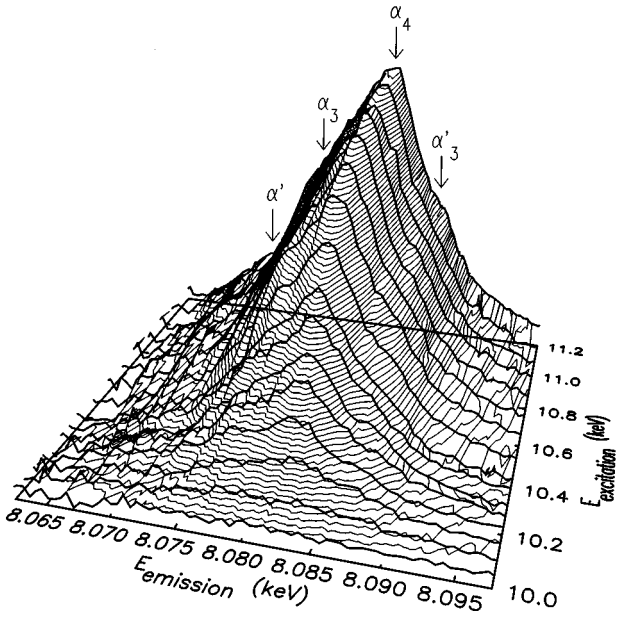

FIG. 1. The Cu $K\alpha_{3,4}$ satellite spectrum variation with excitation energy . The four previously observed features are marked by arrows and by the conventional notation. Note the continuous increase from threshold at ~10 keV to saturation at ~11 keV.

The data sets obtained after the correction and $K\alpha_1$ substraction described above were considered to be the pure satellite spectra and were used for the further analysis and the fits described below.

III. RESULTS AND DISCUSSION

A. Introduction

The evolution of the $K\alpha_{3,4}$ satellite spectrum, E_{emission}, with excitation energy, $E_{\text{excitation}}$, from the threshold at ~ 10 keV up to saturation at ~ 11.2 keV is summarized in Fig. 1, where the four previously identified features [24], due to highly overlapping individual emission lines, are also marked. The overall shape of the ridge is that of a monotonically increasing saturation curve. A closer inspection of the individual measured spectra, marked by heavy lines in Fig. 1, reveals that virtually all of those above $E_{\text{excitation}} \approx 10\,080$ eV have the same shape. As shown in Fig. 2, when normalized to their peak intensity, these spectra overlap almost perfectly. The spectra differ therefore only by an overall intensity factor, but not in shape. Deviations from this perfect overlap, indicating shape changes, are observed only for $E_{\text{excitation}} \leqslant 10\,080$ eV, about 70 eV above the threshold. This is demonstrated by the $E_{\text{excitation}} = 10\,050$ eV spectrum shown in Fig. 2, which is distinctly different from the other three. Its two-peak structure results from a reduction in the intensity of the α_4 line relative to the α_3 one. The excitation energy range from threshold to saturation consists, therefore, of two spectral evolution regimes. In the first (denoted TR for ''threshold regime'' in the following), extending from threshold at ~10 010 eV up to ~10 080 eV, both the shape of the spectrum and its intensity vary considerably, mostly because of the different thresholds of the various features, but also because of different intensity growth rates of the individual lines with excitation energy. In the second regime

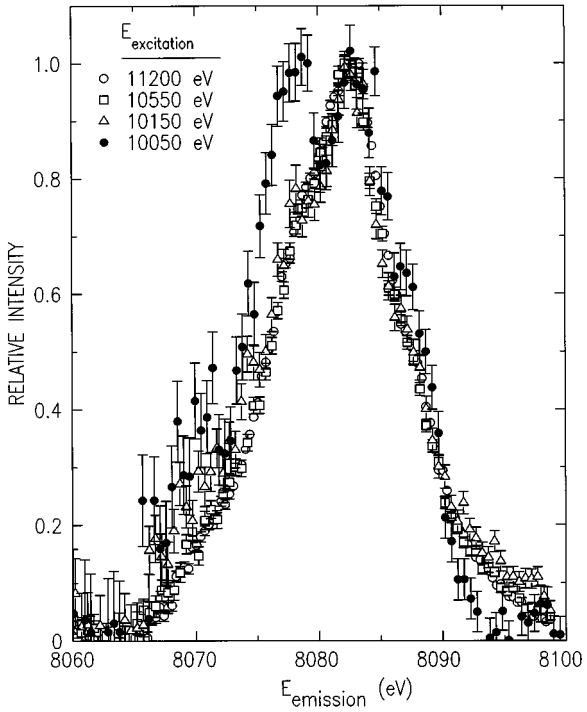

FIG. 2. The $K\alpha_{3,4}$ spectra for the excitation energies listed, each scaled to its peak value. The excellent overlap for spectra above ~10 080 eV demonstrates their identical shape. The shape variations occurring below that limit are examplified by the double-peaked $E_{\text{excitation}} = 10\,050$ eV spectrum.

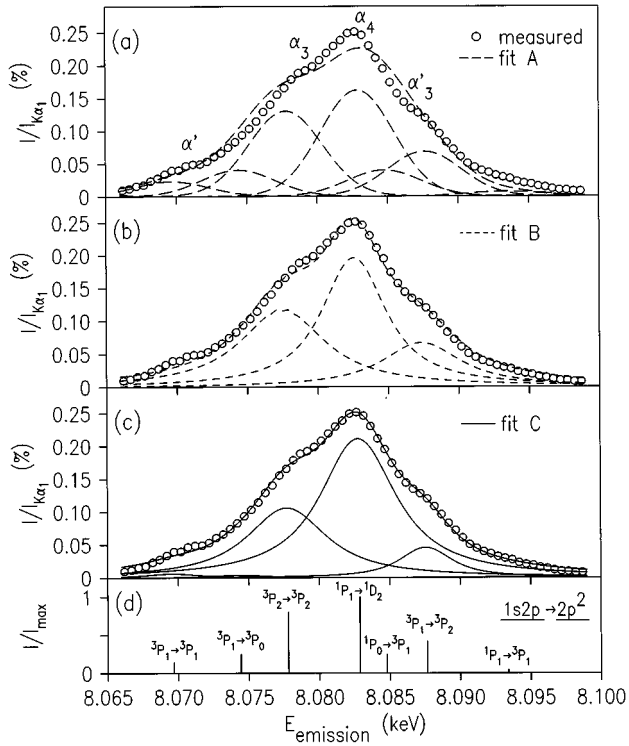

FIG. 3. Theoretical fits of the $K\alpha_{3,4}$ spectrum in the growth regime (GR) by the *ab initio* relativistic Dirac-Fock calculated $\underline{2p}$ spectator transition $\underline{1s2p} \rightarrow \underline{2p}^2$ (lowest frame). $I/I_{K\alpha_1}$ denotes the peak intensity divided by that of the Cu $K\alpha_1$ line. The various fits, showing increasingly better agreement with the measured spectrum, are discussed in the text, as are the assignments of the four observed features to individual transitions.

(GR for ''growth regime''), from ~10 080 eV up to saturation at ~11 000 eV, the spectral shape is already fully developed and only the intensity of the satellite complex as a whole increases in a monotonic, but nonlinear, way. We now discuss the results obtained for each of these two regimes in some detail.

B. The growth regime

The main issues in the GR regime, namely, the individual transitions underlying the spectrum, and the variation of the overall intensity with excitation energy, are addressed in this section. Points already discussed in our recent Letter [3], will be mentioned only briefly.

1. The transitions underlying the $K\alpha_{3,4}$ spectrum

In Fig. 3 we plot the *ab initio* calculated lines corresponding to the $\underline{2p}$ spectator transition $\underline{1s2p} \rightarrow \underline{2p}^2$, which was suggested as early as 1927 [24,32] to give rise to the $K\alpha_{3,4}$ spectrum. Although the atomic number of Cu is high enough for the intermediate, rather than pure LS, coupling to apply, the calculated levels are marked for convenience by their largest LS components. The overall alignment of the calculated and measured spectra is good, and the four main features, $\alpha', \alpha_3, \alpha_4$, and α_3' can clearly be identified with the $^3P_1 \rightarrow {}^3P_1, {}^3P_2 \rightarrow {}^3P_2, {}^1P_1 \rightarrow {}^1D_2$, and $^3P_1 \rightarrow {}^3P_2$ transitions. Note that at most only 7 out of the calculated 14 transitions in the full $\underline{1s2p} \rightarrow \underline{2p}^2$ multiplet contribute to the measured spectrum. The calculated lines at $\geqslant$8098 eV, above the range measured here, are too weak to be observed, and the (only slightly stronger) lines below ~8060 eV are at a region where the $K\alpha_1$ line's slope, and intensity, are too high to allow a meaningful separation of the small contribution of these lines, as was verified experimentally.

To obtain a more quantitative evaluation, we have used the calculated multiplet, with a Lorentzian representing each transition, to fit the measured spectrum. In all fits a single energy shift Δ of the whole calculated multiplet relative to the measured spectrum was allowed. This shift, usually no more than 1–2 eV in our DF calculations, comes mostly from residual inaccuracies in the *ab initio* calculation of the relativistic shifts of the energy levels, particularly those involving the K shell. The finite instrumental window function was represented by convoluting the calculated curve by a Gaussian of a fixed half width at half maximum (HWHM) of 0.8 eV. In Fig. 3 three types of fits, with increasing number of free parameters, are presented. Fit A employed a single width common to all the multiplet lines, and only this width, a single intensity scale factor and the shift Δ were refined in the fit. The as-calculated relative intensities of the lines were therefore preserved. Fit B allowed an individual width to each line, but the relative integrated intensities of the lines were fixed at the calculated values. Finally, fit C allowed these relative intensities to vary as well and only the individual line positions within the multiplet were held fixed. The corresponding fit values are given in Table I. Note first the small shift $\Delta \approx 1$ eV for all fits, showing the calculated energies to be accurate, and lending support to both the assignment of the spectrum to $\underline{2p}$ spectator transitions and to

TABLE I. Fit of the theoretically calculated transitions to the measured spectrum. Energies are in eV and integrated intensities in percents of the total spectral intensity. The fitted shifts between calculated and measured spectra are −1.0, −1.3, and −1.1 eV for fits *A*, *B*, and *C*, respectively. For discussion see text.

	Transition						
	$^1P_1\rightarrow{}^3P_1$	$^3P_1\rightarrow{}^3P_2$	$^1P_0\rightarrow{}^3P_1$	$^1P_1\rightarrow{}^1D_2$	$^3P_2\rightarrow{}^3P_2$	$^3P_1\rightarrow{}^3P_0$	$^3P_1\rightarrow{}^3P_1$
Energy							
Calculated	8094.4	8088.7	8085.8	8083.9	8078.8	8075.4	8070.7
Integ. intensity							
Calc., fits *A* and *B*	1.5	14.5	8.6	34.4	27.5	8.6	4.8
Fit *C*	0.2	8.5	0.0	58.5	30.8	0.8	1.2

the need for a full relaxation between the excitation and emission processes in the calculations. The agreement of even the most restricted fit *A* with experiment is good, indicating no other contributions to the spectrum. Indeed, attempts to include contributions from the calculated $2s$ spectator transitions $1s2s\rightarrow 2s2p$ invariably reduced their intensity to zero [3]. This is in line with the approximately fivefold lower shake probability calculated for a $2s$ electron, as compared to a $2p$ one, to accompany a $1s$ vacancy production [33]. The very strong Coster-Kronig transition $1s2s\rightarrow 1s2p3l$, which depopulates the $2s$ spectator state very fast, further reduces any possible $2s$ spectator contributions to the spectrum [6,28].

From fits *B* and *C* in Fig. 3 it is clear that the three transitions $^3P_2\rightarrow{}^3P_2$, $^1P_1\rightarrow{}^1D_2$, and $^3P_1\rightarrow{}^3P_2$ dominate the spectrum, with only minor contributions from the weaker transitions. Thus, only the contributions of these three lines can be determined with confidence by the fitting procedure from the highly overlapping and feature-poor measured spectrum. The fitting code practically eliminates the contributions of the other lines by reducing their amplitudes to zero in fit *C*, where the integrated intensities are allowed to vary. In fit *B*, where the integrated intensities (proportional to the product of the width and amplitude of each line) are fixed, the amplitudes of the weaker lines are reduced to almost zero by increasing their widths to unphysically large values. Comparing the calculated and fitted integrated intensities in Table I shows that while the three strongest calculated lines are also the three strongest fitted lines, the calculated and fitted intensity distributions among the lines differ considerably. The strongest $^1P_1\rightarrow{}^1D_2$ line gains considerable intensity, the second strongest $^3P_2\rightarrow{}^3P_2$ line intensity remains as calculated, and all other lines are considerably reduced from their calculated values. This indicates that while our single configuration, sudden-approximation RDF calculation captures the essentials of the spectrum, further effects, such as slightly less-than-full relaxation and/or final- and initial-state correlations, need be considered to improve the agreement with experiment.

2. Intensity variation with excitation energy

Figure 4 shows the evolution of the integrated intensity of the measured spectra from threshold to saturation. Two separate sets of measurements, done at different times after separate alignment procedures, denoted ''set 1'' and ''set 2,'' which agree well with each other, are presented. The continuous rise of the curve from zero at threshold clearly marks the satellites as originating in a shakeoff, rather than a shakeup, process, since the latter results in an intensity jump at the threshold [3,6,15,21]. This is in full accord with our expectation, discussed above, as well as the $\leqslant 1\%$ contribution predicted [3] for shakeup in our case, as extrapolated from RDF calculations for Ar [34] and Kr [23]. The high-energy saturation limit of 0.63% of the $K\alpha_1$ intensity is in good agreement with previous measurements [24,25,35] and calculations [6,36]. Note also that no outstanding features are observed in the intensity curve at ~10 170 eV, the calculated threshold for the simultaneous excitation of a $1s$ plus a $2s$ electrons, further supporting the conclusion above of a negligible $2s$ spectator contribution to the spectrum.

As observed in the figure, the energy range required to reach saturation, ~1 keV, or 10% of the threshold energy, is considerably larger than the corresponding ~70 eV and 2% measured for the Auger shakeoff [21] and shakeup [15] satellites accompanying the $1s$ photoionization in Ar. On the other hand, Parratt's [37] early measurements of the Ti $K\alpha_{3,4}$ satellite intensity variation with x-ray tube voltage, yield a range of ~3 keV, or ~50% of the threshold energy, much larger than found here. Since all three spectra originate in

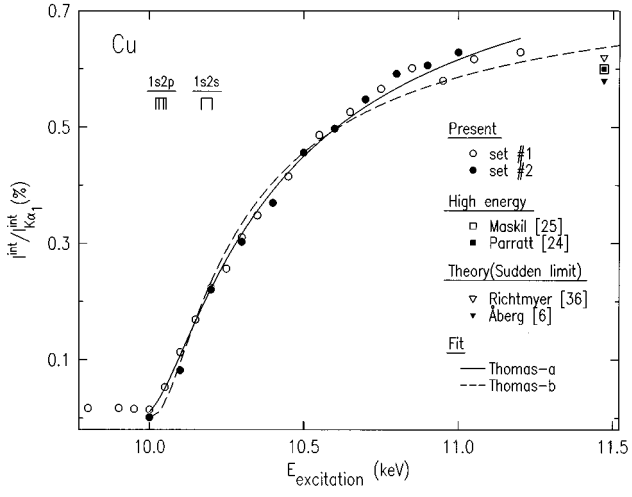

FIG. 4. The overall integrated intensity variation of the satellite spectrum in the GR regime. Several previously measured, and calculated, high-energy limits of the intensity are also shown, as are the relativistic Dirac-Fock calculated thresholds for the $2p$ and $2s$ spectator levels. Fits to the Thomas model are discussed in the text. The relevant references, from the list at the end of the paper, are given in square brackets.

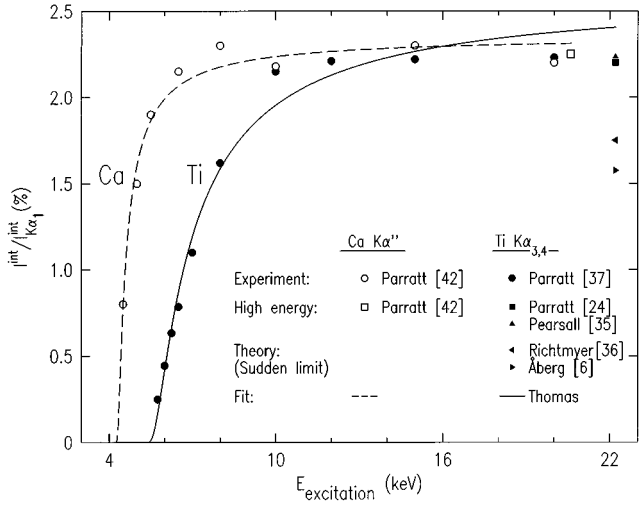

FIG. 5. The overall integrated intensity variation of the Ti $K\alpha_{3,4}$ (a $2p$-spectator transition) and the Ca $K\alpha''$ (a $3p$-spectator transition) satellite spectra, from their respective threshold up, as measured by Parratt [24,37]. Although they look reasonable by eye, the corresponding Thomas model fits yield parameters that deviate considerably from measurements and expectations. For discussion see text.

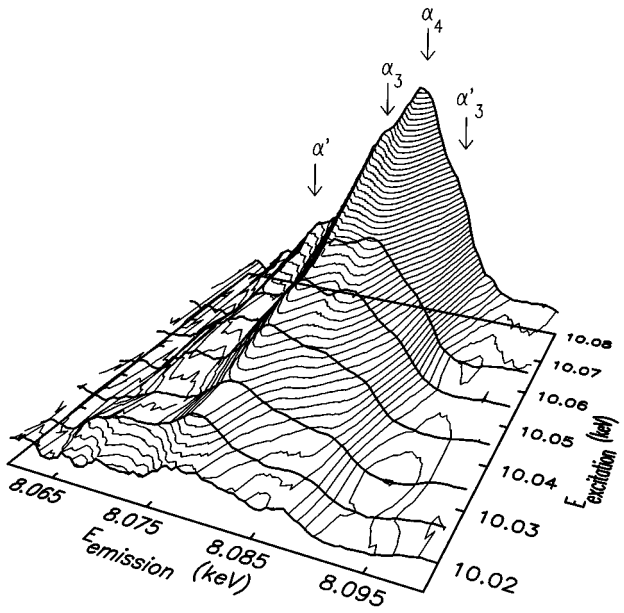

FIG. 6. The near-threshold evolution of the Cu $K\alpha_{3,4}$ satellite spectrum with excitation energy. At the lowest energies the α_3 ridge is the strongest, while above its $\sim$10 030 eV threshold the α_4 ridge rises fast to dominate the spectrum.

shake processes accompanying a $1s$ photoionization, for which the Thomas model should be valid, and considering the recent success of that model in accounting for the Ar Auger satellite measurements [15], we attempted to fit our data, and Parratt's Ti one, by the intensity curve predicted by this model.

The Thomas model [10] can be expressed in a closed form, if we accept the convenient *ad hoc* assumptions of a Gaussian time dependence for the Hamiltonian's time derivative and a constant velocity for the ejected photoelectron while within the bounds of the atom [9]. Under these assumptions the satellite intensity I_{Thomas} varies as

$$I_{\text{Thomas}} = I_\infty \exp\left(\frac{-r^2 \Delta E^2}{15.32 E_{\text{ex}}}\right), \tag{1}$$

where r is the radius, in Å, of the shell in which the shakeup occurs ($2p$, in our case) and I_∞ is the intensity at the high-energy, sudden approximation limit. $E_{\text{ex}} = E_{\text{excitation}} - E_{\text{threshold}}$ is the excess energy of the exciting photon above the excitation threshold $E_{\text{threshold}}$, and ΔE is the shakeup energy. In our case, $\Delta E \sim 1002$ eV, which can be obtained through the $Z+1$ approximation [38] from the measured [39] Zn L_{III} ionization energy of 1021.8 eV, reduced by 2% as suggested by Parratt [24]. A very close value is also obtained by taking the difference between the RDF-calculated $1s$ and $1s2p$ energies. The parameters varied in the fit are I_∞, r, and $E_{\text{threshold}}$. The fit results are denoted as ''Thomas-a'' in Fig. 4 and yield values of $0.88 \pm 0.03\%$, 0.07 Å, and 9911 ± 17 eV, respectively, for the three parameters. While the overall agreement of the data and the fitted model is good, the values obtained for the parameters do not agree too well with other, independent data. Specifically, the I_∞ is about 30% higher than the $\sim$0.63% measured here, and also previously, for the sudden limit. Heiser *et al.*'s [15] fit of the Thomas model to their Ar photoelectron shakeup data also overshoots the measured sudden limit value of Armen *et al.* [21] by $\sim$20%. In contrast with these deviations of I_∞ for our Cu data and Heiser's Ar data, excellent agreement was obtained for Ne [15,14,40] between the Thomas-fitted $I_\infty = 5.12 \pm 0.03\%$ and the measured [41] 5.15%. An attempt to improve the agreement here with the sudden limit was made by adding to our fitted data set a number of ''measured'' points, having the sudden limit value, at energies above the highest measured in this study, 11.2 keV. This resulted in the line denoted ''Thomas-b'' in the figure and $0.76 \pm 0.03\%$, 0.064 Å, and 9970 ± 25 eV for the three parameters. While I_∞ agrees now better with the experiment, the shape of the curve is in markedly worse agreement with the measurements near threshold. The fact that the functional form of the model cannot reproduce well the shape near threshold and the high-energy limit simultaneously indicates that the probable cause for the deviations is the *ad hoc* choice of a Gaussian time dependence for the Hamiltonian's derivative. Foregoing this choice requires numerical solution, rather than a close-form one, of the time-dependence equations as shown by Thomas [9]. It may, however, yield a better agreement with the data both in our and in Heiser *et al.*'s case. Note that the agreement between the measured threshold, $\sim$10 010 eV, and the fitted one is not too good either, although the ''Thomas-b'' fit is reasonably close. The radius of the $2p$ shell obtained from the fits is also somewhat lower, though not by much, than the 0.1 Å calculated by us using the RDF code.

Finally, we have also fitted the Thomas model to the early Ti $K\alpha_{3,4}$ and Ca $K\alpha''$ satellite data of Parratt [37,42], measured as a function of the x-ray tube voltage and shown in Fig. 5. The same difficulties discussed above are observed. For the Ti data the actual saturation is faster than is possible to reproduce with the analytic Thomas model, Eq. (1). The fitted threshold energy, 5260 ± 170 eV, is lower than the cal-

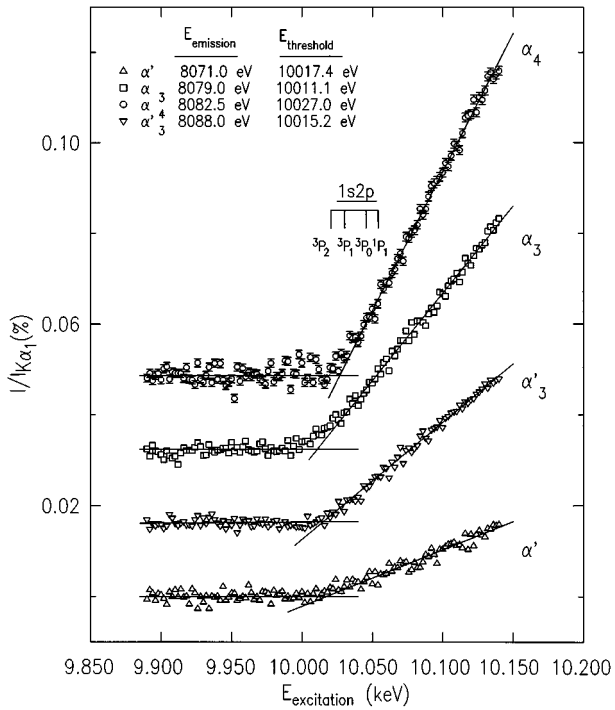

FIG. 7. The nominal thresholds for the various features, as determined from intersections of straight lines fitted, below and above the threshold, to curves of the emission intensity variation with excitation energy. These were measured with the emission energy fixed in turn at the position of the features marked in Fig. 1. The curves are shifted from each other for clarity. The RDF-calculated thresholds for shakeoff are also shown.

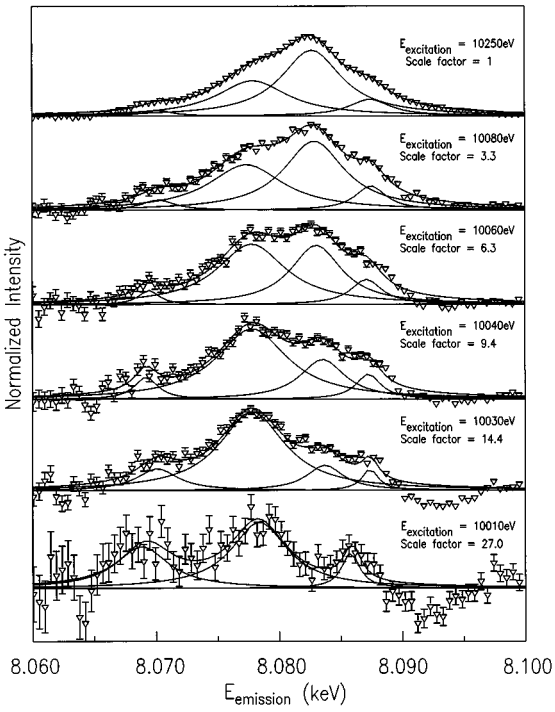

FIG. 8. The measured spectra in the near threshold (TR) region, for several excitation energies, each normalized to its maximum by the scale factor listed. Fits to a sum of four Lorentzians, and the individual Lorentzians, are shown in solid lines. Note the roughly constant widths and positions of the lines, and the increase of the α_4 line from zero below threshold to domination at ~10 080 eV.

culated, and the measured ones of ~5500 eV. $I_\infty = 2.60 \pm 0.12\%$ is about 20% higher than the measured [35,24] 2.2%. The fitted $2p$ shell radius of 0.286 Å, calculated with [39] $\Delta E = 505$ eV, is almost twice as large as our RDF-calculated value of 0.15 Å. For the Ca $K\alpha''$ satellite, which has been identified in several studies [42–44] to originate in the $3p$ spectator transitions $1s3p \rightarrow 2p3p$, the fit in the figure appears by eye to be better than for the Ti data. The fitted high-energy limit $I_\infty = 2.35 \pm 0.18\%$ is in very good agreement with the high-energy limit of 2.25%, measured in the same study [42]. However, this is achieved at the cost of obtaining a fitted $3p$ shell radius of $r = 2.38$ Å (for [39] $\Delta E = 28.3$ eV), fourfold larger than the RDF calculated 0.59 Å. The fitted threshold energy, $E_{\text{threshold}} = 4230 \pm 120$ eV, is much larger than the 4066.8 eV obtained through the $Z+1$ approximation from photoelectron spectroscopy energy levels [39], and Parratt's [42] estimate of 4070 eV. In fact, Parratt used this threshold estimate as the basis of his identification of the α'' line with the $3p$ spectator transition. With the fitted value, which lies half way between the $3p$ spectator threshold and that of the $2p$ at [39] 4430 eV, his identification would not have been supportable. The large deviations of the fitted values from the experimental and calculated ones both in Parratt's early study as well as that presented here, reflect, again, the severe approximations used in the model as discussed above. These result clearly indicate the need for more accurate calculations in the adiabatic regime, preferably without employing the simplifying assumptions discussed above.

C. The threshold regime

1. Determination of the thresholds

An overview of the evolution of the spectra in the near-threshold region is shown in Fig. 6. A careful examination shows the dominance of the $K\alpha_3$ feature near threshold, the subsequent opening of the $K\alpha_4$ excitation channel near 10 030 eV, and its fast increase to dominance over the $K\alpha_3$ line at 10 080 eV. The thresholds and evolution of the two weaker features $K\alpha'$ and $K\alpha'_3$ are less clear in this figure. However, scans of $E_{\text{excitation}}$ while keeping E_{emission} fixed at each of the features in turn, should allow an accurate determination of the threshold of these features. Such scans are shown in Fig. 7. The most outstanding feature of these inscans is that even on this highly magnified scale, where intensity variations of $\leqslant 5\times 10^{-5}$ of the $K\alpha_1$ line should be clearly discernible, no abrupt intensity jumps are observed for any of the features at threshold, and the intensity rises from zero continuously, smoothly, and linearly, within the accuracy of this experiment. This pure shakeoff behavior is a striking corroboration of the prediction, discussed above, that inner-shell shake processes should be increasingly dominated by the *shakeoff* , rather than the shakeup, effect. The growth of each feature over the limited $E_{\text{excitation}}$ range shown is highly linear, although over the full adiabatic range it is not, as shown in Fig. 4. The RDF-calculated thresholds of the features, shown in the figure, are in reasonable agreement with the measurements, although upshifted by 5–10 eV. They also correspond well to the transition assignments of the various features in Fig. 3. The linear energy depen-

TABLE II. Resolution of the $K\alpha_{3,4}$ spectrum into 4 component lines, for the excitation energies indicated. E_0, Γ (both in eV), and I_0 (in arbitrary units) are the energy position, Lorentzian width, and intensity, respectively, of each line. Second-line entries are the uncertainties in the values listed in the corresponding values in the first line.

Line	Parameter	$E_{excitation}$ (eV)								
		10 010	10 022	10 030	10 040	10 045	10 050	10 060	10 080	10 250
α_3'	E_0	8085.8	8086.5	8087.5	8087.3	8087.2	8087.9	8087.1	8087.5	8087.5
		0.4	0.4	0.3	0.3	0.3	0.3	0.4	0.2	0.2
	Γ	0.72	1.27	0.7	1.15	1.26	1.35	1.54	1.40	1.70
		0.53	0.60	0.59	0.58	0.48	0.50	0.69	0.41	1.9
	I_0	1.40	1.45	1.61	2.71	4.01	3.17	4.30	7.30	1.40
		0.62	0.39	0.68	0.63	0.72	0.59	1.0	1.1	0.62
α_4	E_0		8082.6	8083.8	8083.6	8083.4	8083.6	8083.0	8083.0	8082.7
			0.7	0.5	0.3	0.2	0.2	0.2	0.2	0.1
	Γ		1.0	1.8	2.19	2.30	2.64	2.53	3.06	3.11
			1.44	1.20	0.81	0.68	0.50	0.68	0.48	0.11
	I_0		0.68	1.82	4.21	7.40	7.71	10.1	21.2	67.7
			0.46	0.45	0.63	1.10	0.60	1.20	2.00	4.00
α_3	E_0	8078.4	8077.2	8077.8	8077.9	8078.3	8077.6	8077.8	8077.4	8078.0
		0.3	0.2	0.3	0.3	0.4	0.2	0.3	0.4	0.3
	Γ	2.66	3.17	3.26	3.63	3.92	3.41	3.23	4.11	3.85
		0.63	0.42	0.54	0.41	0.45	0.41	0.52	0.63	0.30
	I_0	2.47	5.12	5.62	7.66	9.41	8.74	10.00	14.40	36.30
		0.29	0.25	0.34	0.48	0.91	0.53	1.00	1.80	3.90
α'	E_0	8068.9	8069.2	8070.1	8069.2	8069.3	8069.9	8069.8	8069.9	8070.0
		0.6	0.3	0.6	0.3	0.8	0.4	0.6	0.4	0.3
	Γ	3.50	2.50	2.40	1.26	1.30	2.23	2.00	1.58	1.29
		1.30	0.62	1.10	0.45	1.30	0.72	1.10	0.84	0.47
	I_0	1.55	2.26	1.50	2.29	0.94	2.13	1.82	2.68	5.00
		0.26	0.29	0.37	0.49	0.54	0.38	0.64	0.79	1.00

dence of the intensity was employed to derive the thresholds listed in the figure, calculated from the intersections of straight line sections fitted to the data above and below the threshold. The small deviations of these values from those obtain from similar, but lower-statistics, measurements in Ref. [3] reflect the few eV accuracy achievable by this method. In view of these, the agreement between the measured difference of ~16 eV of the $K\alpha_3$ and $K\alpha_4$ thresholds, the RDF-calculated 25 eV difference of the corresponding $^3P_2$-$^1P_1$ levels and the ~20 eV separation of the $2p_{1/2}$ and $2p_{3/2}$ subshell energies in Cu, is not too bad. The positions of the α' and α_3' thresholds, in between those of the α_3 and α_4 lines, also corresponds well to their assignment to the transitions originating in the $^3P_1$ initial level, although with the accuracy available, not much significance can be attached to the deviations of the calculated values from the measured ones. Note finally that the thresholds derived here as the intersections of the straight lines are nominal only, in the sense that the actual data points may lie slightly above these lines at the intersection, and even somewhat below it, and still evolve with $E_{excitation}$. This is particularly clear for α_3 where the measured intensity shown in the figure near the nominal threshold is markedly rounded, and the data points lie above the fitted straight lines. Indeed, as we show below, even at $E_{excitation}$=10 010 eV, just at the nominal threshold, there is still some intensity in this line. However, the straight

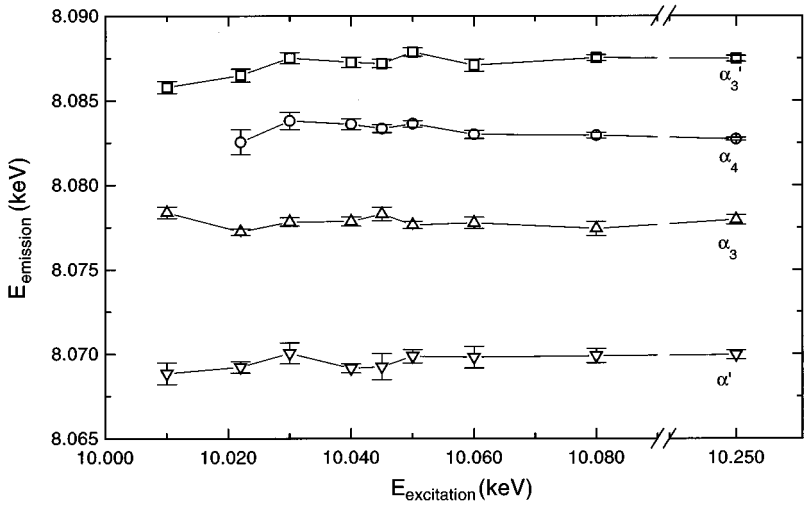

FIG. 9. The variation of the individual line positions with excitation energy near threshold. Note the almost fixed positions of all lines. The small downshift of the α_4 line just below threshold (10 022 eV) is disscused in the text.

line intersections are still the best choices for the nominal thresholds for comparing with theory as done above. This is because the measurement errors due to the high $K\alpha_1$ background and the gradual variation of the intensity of the lines do not allow the extraction from the outscans of a definite $E_{\text{excitation}}$ value at which a given line disappears, particularly for the weak α' and α_3' lines.

2. The shape evolution of the spectrum

Several of the spectra measured in this near-threshold TR regime are shown in Fig. 8. Each spectrum is normalized to its maximal intensity, so that the weakest spectrum, at $E_{\text{excitation}}=10\,010$ eV, is about 30fold less intense than the strongest one, at $E_{\text{excitation}}=10\,250$ eV. This intensity decrease, and the high background due to the $K\alpha_1$ tail, effectively prevented meaningful satellite spectrum extraction at lower $E_{\text{excitation}}$ values. Note that for reasons mentioned above, remnants of some of the lines are still observed at the lowest $E_{\text{excitation}}$ spectrum, measured at the lowest nominal threshold, that of α_3. The variation of the shape with $E_{\text{excitation}}$, observed in the figure, is marked and rapid. The main effect observable by eye is the higher threshold of the singlet $^1P_1$, the originator of the α_4 line, as compared with the triplet ^3P, which gives rise to the α_3, α', and α_3' lines. For a better assessment of the individual line evolution, the measured spectra were fit by Lorentzians. In this highly adiabatic limit the validity of the sudden approximation RDF calculations, and hence the description of the spectrum by 7 lines as discussed above, is questionable. The data indicate only 4 underlying lines. We have, therefore, used only 4 Lorentzians in the fit. Because of the good analyzer resolution, and the high-quality fit achieved, no convolution with the instrumental function was applied in these fits. Attempts to include more Lorentzians, at positions indicated by the RDF calculations, did not improve the fits. The same is true for fits where the positions and/or half-widhts were restricted to the values of the fully developed spectrum. In fact, a distinct degradation was observed in the restricted fits for the very-near-threshold spectra. Thus, all three parameters of each Lorentzian (width, height, position) were allowed to vary in the fit.

The individual Lorentzians and their fitted sums are compared with the measured spectra in Fig. 8, and the resultant fit parameters listed in Table II. The fit of the $E_{\text{excitation}}=10\,010$ eV spectrum confirms that although there is a small contribution of the α_3, α', and α_3' lines, which is not surprising in view of the few-eV energy spread in $E_{\text{excitation}}$ and the proximity of their thresholds, no contribution is observed from the α_4 line, whose nominal threshold is $\sim$17 eV higher, hence the missing values in Table II for the α_4 line at this excitation energy. Just above its nominal threshold a small contribution of this line appears ($E_{\text{excitation}}=10\,030$ eV), and increases steadily, faster than the other lines, to dominate the spectrum at $E_{\text{excitation}}=10\,080$ eV. A comparison of the shape and the relative intensities of the resolved lines in Fig. 8 for $E_{\text{excitation}}=10\,080$ eV and 10 250 eV demonstrates that at 10 080 eV the shape is already saturated and does not change further. The positions of the individual lines, plotted in Fig. 9, are virtually constant, when the error bars, obtained from the fit, and the spread in nearby points are considered. The only (rather weak) exception may be the α_4 position at $E_{\text{excitation}}=10\,020$ eV, slightly below the nominal threshold, which is $\sim$1.2 eV lower than its immediate neighboring points, just barely outside the combined error bars. The Lorentzian width obtained at this energy for this line is also lower than those of the same line at higher energies, as shown in Fig. 10. Nevertheless, in view of the large uncertainties, no support can be drawn from these observations for the existence of a resonant Raman (RR) effect [45] for this line, in spite of the fact that the two main signatures of this effect are a linear shift of the line position towards lower energies below threshold, and a narrowing of the linewidth when approaching the threshold from below or above. None of the other lines shows signs of similar effects, although the 10 010-eV measurements are also below threshold for the α' and α_3' lines. Clearly, much more accurate measurements are required to decide whether the RR effect exists for the transitions studied here.

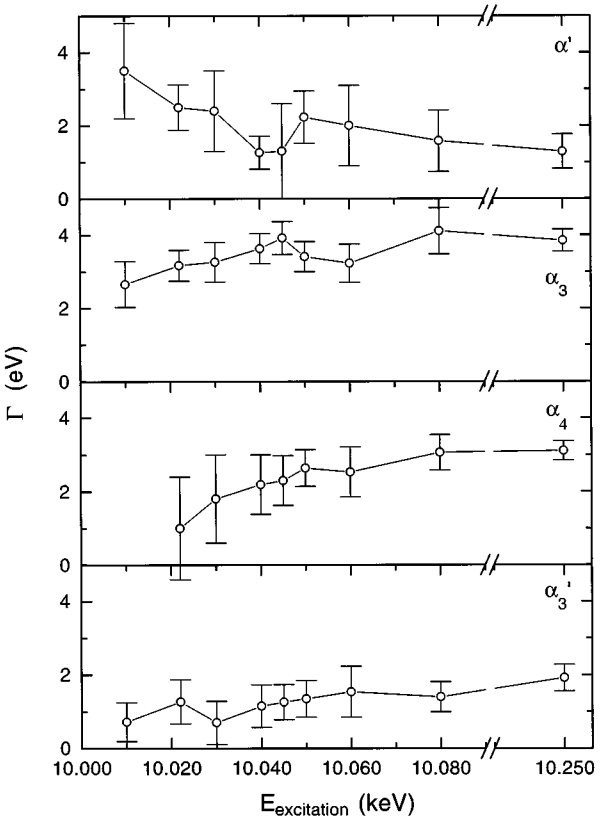

FIG. 10. The variation of the Lorentzian widths of the individual lines with excitation energy near threshold. The only possible sign of line narrowing is at the threshold of the α_4 line. Otherwise the widths are constant within the errors shown.

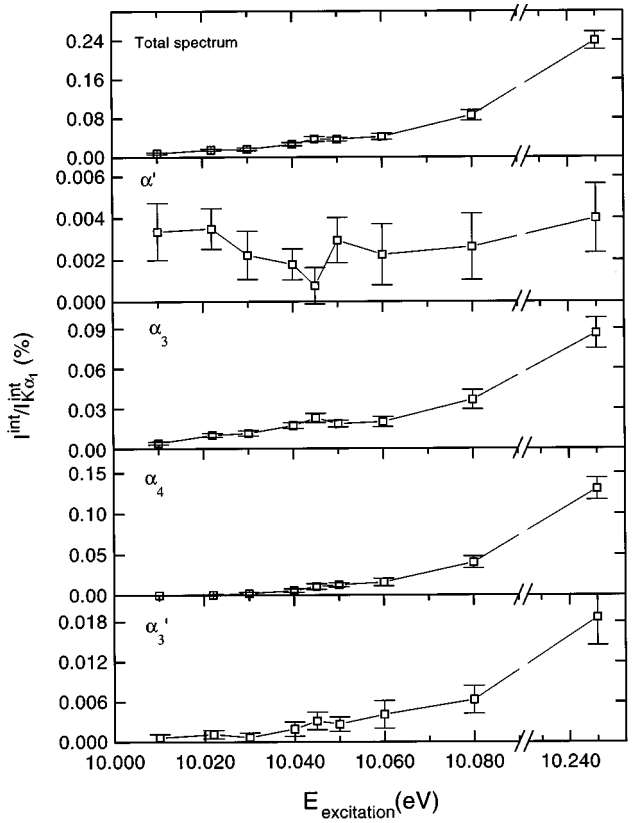

FIG. 11. The variation of the integrated intensities of the individual lines, and the full spectrum, with excitation energy near threshold. The higher threshold of the α_4 line, as compared to the α_3 line, and the intermediate α_3' threshold are clearly observed. The constant intensity of the α' line is probably an artifact, as discussed in the text.

The widths of all other lines in Fig. 10 seem reasonably constant within the measurement errors, and equal to their sudden limit values. The narrower widths of the weaker α' and α_3' lines , as compared to the strong α_3 and α_4, and the $\sim$1 eV broader α_3 line as compared to α_4, seem to be consistent, and real, effects for which no explanation can be offered at present. Finally, the integrated intensities of the individual lines on a scale relative to that of the $K\alpha_1$ line are plotted in Fig. 11. They rise gradually from zero, without any abrupt jumps even on scales of a few parts in 10^5, confirming again the pure shakeup nature of these transitions. The seemingly anomalous behavior of the α' line, showing a roughly constant intensity with excitation energy, is most probably an artifact, reflecting the difficulty of separating out the contribution of this weakest line, as also shown by the large error bars in the plot. The faster growth of the α_4 line as compared to the α_3 line is clearly demonstrated by the variation of the ratio of their intensities with excitation energy, shown in Fig. 12. The ratio saturates fast, and its value at $E_{\text{excitation}}=10\,080$ eV already agrees well with both the calculated RDF value and the ratio as obtained from the measurements for $E_{\text{excitation}}=10\,250$ eV and up. This is as expected from the full saturation of the spectral shape at $E_{\text{excitation}}=10\,080$ eV. Assuming a linear growth from zero at their respective thresholds for both intensities yields the line marked ''linear growth model'' in the figure, which agrees well with the measurements.

IV. CONCLUSION

The two-regime behavior of the Cu $K\alpha_{3,4}$ satellite spectrum, where near the threshold both the shape and intensity, and further away only the intensity, but not the shape, of the

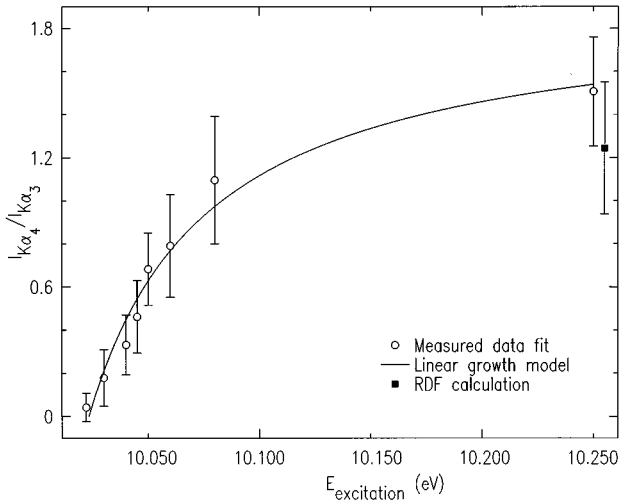

FIG. 12. The intensity ratio of the α_4 line to that of the α_3 line near threshold, demonstrating the faster growth of the α_4 line. The linear growth model assumes a smooth linear increase of the intensities from threshold, and agrees very well with the near-threshold data and the calculated high-energy RDF value.

spectrum vary with excitation energy, reported here, is a novel effect. In the absence of other detailed studies of this type, it is not clear whether this behavior is general, restricted to medium-Z, to the $3d$ transition elements, or even peculiar to copper only. On the theoretical side, the Thomas model for the intensity growth in the adiabatic GR regime, which was expected to be fully applicable here since both the shakeoff and the primary electrons come from inner shells, did not reproduce well the experimental results. A first step towards improving the agreement is to dispense with the Gaussian time-dependence approximation, and/or take the time-dependent perturbation theory to orders higher than the first. This, of course, carries a cost of having to solve the equations numerically, rather than obtaining a convenient closed-form solution. Also, *ab-initio* calculations of the spectral shape near threshold (the TR regime in our case), and its evolution with excitation energy, received virtually no attention to date, perhaps due to the absence of experimental results against which the theory could be tested. Basic questions like the importance of initial- and final-state correlations, the detailed rearrangement dynamics of the shells, the interactions between the slow moving ejected photoelectron, and the relaxing atom, etc. should in principle be accessible in this regime by combined theoretical and experimental studies. Above all, however, a larger body of experimentally derived data, like the one presented here, on the evolution from threshold to saturation of emission lines, both diagram and satellite, is indispensable for going beyond the simplified, independent electron picture of the atom and the frozen-core–sudden approximation description of atomic excitation processes.

ACKNOWLEDGMENTS

This work was supported in part by The Israel Science Foundation, Jerusalem (M.D.), the Academy of Finland under Grant No. SA-8582 (K.H.), and the Max Planck Society (E.F.). Brookhaven National Laboratory is supported by the U.S. Department of Energy under Contract No. DE-AC02-76CH00016.

[1] *Atomic Inner-Shell Physics*, edited by B. Crasemann (Plenum, New York, 1986).
[2] B. Crasemann, J. Phys. (France) Colloq. **48**, C9-389 (1987); V. Schmidt, Rep. Prog. Phys. **55**, 1483 (1992).
[3] M. Deutsch, O. Gang, K. Hämäläinen, and C.C. Kao, Phys. Rev. Lett. **76**, 2424 (1996).
[4] J. Stöhr, R. Jaeger, and J.J. Rehr, Phys. Rev. Lett. **51**, 821 (1983).
[5] T. Aberg, Phys. Rev. **156**, A35 (1967).
[6] T. Åberg, in *Proceedings of the International Conference on Inner-Shell Ionization Phenomena and Future Applications*, edited by R. W. Fink, S. T. Manson, J. M. Palms, and P. V. Rao (NTIS, U.S. Dept. of Commerce, Springfield, VA, 1972), p. 1509 (U.S. AEC Report No. CONF-720404).
[7] T.A. Carlson and O.M. Krause, Phys. Rev. **140**, A1057 (1965).
[8] J. Tulkki and T. Åberg, J. Phys. B **18**, L489 (1985); J. Tulkki *et al.*, Z. Phys. D **5**, 241 (1987).
[9] T. D. Thomas, J. Electron Spectrosc. Relat. Phenom. **40**, 259 (1986).
[10] T. D. Thomas, Phys. Rev. Lett. **52**, 417 (1984).
[11] E. Vatai, Phys. Rev. A **38**, 3777 (1988); Acta Phys. Hung. **65**, 257 (1989).
[12] U. Becker, R. Hölzel, H.G. Kerkhoff, B. Langer, D. Szostak, and R. Wehlitz, Phys. Rev. Lett. **56**, 1120 (1986).
[13] G.B. Armen, S.H. Southworth, J.C. Levin, U. Arp, T. LeBrun, and M.A. MacDonald, Phys. Rev. A **56**, R1079 (1997).
[14] U. Becker and D.A. Shirley, Phys. Scr. **T31**, 56 (1990).
[15] F. Heiser, S.B. Whitefield, J. Viefhaus, U. Becker, P.A. Heimann, and D.A. Shirley, J. Phys. B **27**, 19 (1994).
[16] K. Hämäläinen, D. P. Siddons, J. B. Hastings, and L. E. Berman, Phys. Rev. Lett. **67**, 2850 (1991).
[17] C.C. Kao, W.A. Caliebe, J.B. Hastings, K. Hämäläinen, and M.H. Krisch, Rev. Sci. Instrum. **67**, 1 (1996); K. Hämäläinen, M. Krisch, C.C. Kao, W. Caliebe, and J.B. Hastings, *ibid.* **66**, 1699 (1995).
[18] ''Atomic Physics with Hard X-Rays from High Brilliance Synchrotron Light Sources,'' edited by S. Southworth and D. Gemmell, Argonne National Laboratory Report No. ANL/APS/TM-16, 1996.
[19] R. D. Deslattes, R. E. LaVilla, P. L. Cowan, and A. Henins, Phys. Rev. A **27**, 923 (1983).
[20] N. Wassdahl *et al.*, Phys. Rev. Lett. **64**, 2807 (1987); Y. Ma, K. E. Miyano, P. L. Cowan, Y. Aglitzkiy, and B. A. Karlin, *ibid.* **74**, 478 (1995).
[21] G. B. Armen *et al.*, Phys. Rev. Lett. **54**, 182 (1985).
[22] M. O. Krause and C. D. Caldwell, Phys. Rev. Lett. **59**, 2736 (1987).
[23] D. L. Wark, *et al.*, Phys. Rev. Lett. **67**, 2291 (1991); S. J. Schaphorst *et al.*, Phys. Rev. A **47**, 1953 (1993).
[24] L. G. Parratt, Phys. Rev. **50**, 1 (1936); H. J. Edwards and J. I. Langford, J. Appl. Crystallogr. **4**, 43 (1971).
[25] N. Maskil and M. Deutsch, Phys. Rev. A **38**, 3467 (1988).
[26] K.G. Dyall *et al.*, Comput. Phys. Commun. **55**, 425 (1989).
[27] J.W. Cooper, Phys. Rev. A **38**, 3417 (1988); H.P. Saha, *ibid.* **42**, 6507 (1990); M.H. Chen, in *Atomic Inner-Shell Physics* (Ref. [1]).
[28] M. Deutsch, G. Hölzer, J. Härtwig, J. Wolf, M. Fritsch, and E. Förster, Phys. Rev. A **51**, 283 (1995).
[29] E. P. Bertin, *Introduction to X-Ray Spectrometric Analysis* (Plenum, New York, 1978), p. 373.
[30] *International Tables for X-ray Crystallography*, edited by C. H. MacGillavry and G. D. Rieck (Kynoch, Birmingham, 1968), Vol. III, p. 161.
[31] H. Berger, X-Ray Spectrom. **15**, 241 (1986).
[32] M. J. Druyvesteyn, Z. Phys. **43**, 707 (1927).
[33] T. Mukoyama and K. Taniguchi, Phys. Rev. A **36**, 693 (1987).
[34] K. G. Dyall, J. Phys. B **16**, 3137 (1983); see also discussion and references in T. Mukoyama and Y. Ito, Nucl. Instrum. Methods, Phys. Res. B **87**, 26 (1994).
[35] A.W. Pearsall, Phys. Rev. **48**, 133 (1935).
[36] R. D. Richtmyer, Phys. Rev. **49**, 1 (1936).
[37] L.G. Parratt, Phys. Rev. **49**, 132 (1936).

[38] J.P. Desclaux, B. Briancon, J.P. Thibault, and R.J. Walker, Phys. Rev. Lett. **32**, 447 (1974); M. Deutsch, Phys. Rev. A **39**, 3956 (1989).
[39] M. Cardona and L. Ley, *Photoemission from Solids* (Springer, Berlin, 1978); A. Lebugle, U. Axelsson, R. Nyholm, and N. Mȯrtensson, Phys. Scr. **23**, 825 (1981).
[40] P.H. Kobrin, S. Southworth, C.M. Truesdale, D.W. Lindle, U. Becker, and D.A. Shirley, Phys. Rev. A **29**, 194 (1984).
[41] U. Gelius, J. Electron Spectrosc. Relat. Phenom. **5**, 985 (1974).
[42] L.G. Parratt, Phys. Rev. **49**, 502 (1936).
[43] B.L. Scott, Phys. Rev. A **34**, 4438 (1986).
[44] D. Anagnostopoulus and M. Deutsch (unpublished).
[45] P. Eisenberger, P. M. Platzman, and H. Winick, Phys. Rev. Lett. **36**, 623 (1976); T. Åberg and B. Crasemann, in *Resonant Anomalous X-Ray Scattering*, edited by G. Materlik, C. J. Sparks, and K. Fischer (Elsevier, Amsterdam, 1994).